Enhanced radiative cooling of solar cells by integration with heat pipe

Article *in* Applied Energy · February 2022

DOI: 10.1016/j.apenergy.2021.118363

CITATIONS
0

READS
79

5 authors, including:

Salman Ahmed
Shanghai Jiao Tong University
11 PUBLICATIONS **127** CITATIONS
SEE PROFILE

Senji Li
Shanghai Jiao Tong University
3 PUBLICATIONS **8** CITATIONS
SEE PROFILE

Zhenpeng Li
Shanghai Jiao Tong University
14 PUBLICATIONS **305** CITATIONS
SEE PROFILE

Tao Ma
Shanghai Jiao Tong University
93 PUBLICATIONS **3,910** CITATIONS
SEE PROFILE

Enhanced radiative cooling of solar cells by integration with heat pipe

Salman Ahmed[1], Senji Li[1], Zhenpeng Li[1], Gang Xiao[2], Tao Ma[1*]

[1] *Engineering Research Centre of Solar Energy and Refrigeration of MOE, School of Mechanical Engineering, Shanghai Jiao Tong University, Shanghai, China*

[2]*College of Energy Engineering, Zhejiang University, Hangzhou, China*

[*]*Corresponding author e-mail address: tao.ma@connect.polyu.hk*

Abstract

Thermal management of solar cells is of vital importance to maintain adequate electrical efficiency. Lately, radiative cooling (RC) of solar cells has been researched extensively because of its passive nature and structural simplicity. However, commercial solar cells are usually encapsulated with highly emissive glass covers, and therefore the additional potential to reduce the cell temperature through RC is not significant. This study proposes a new system configuration to maximize the RC potential. It consists of a photovoltaic module for electricity generation, an RC module for heat removal to the sky, and a heat pipe for quick and efficient heat transfer between the two modules. A comparative analysis of temperature reduction and efficiency improvement between the proposed and previously studied systems is performed. The influence of input parameters (i.e., solar radiation, ambient temperature, wind speed, atmospheric emissivity, radiator length, and heat pipe resistance) on the system performance is also studied using COMSOL. Results show that in contrast to the conventional glass-coated module, the proposed system gives a maximum cell temperature reduction of 12.86 °C, which corresponds to a 7.25% relative rise in electrical efficiency. The new configuration's enhanced thermal performance supports it as an alternative to the glass-coated or ideally emissive photovoltaic modules. By addressing the challenge of limited radiative sky cooling, researchers can eventually move a step ahead and use this study for the thermal management of other devices and not just solar photovoltaics.

Keywords: Thermal management; Radiative cooling; Heat pipe, Photovoltaic; PV cooling;

Nomenclature

Abbreviations

RC	Radiative Cooling
PV	Photovoltaic
MIR	Mid-Infrared
EVA	Ethyl Vinyl Acetate
HP	Heat Pipe
TPT	Tedlar Polyester Tedlar

Symbols

$A_{wall,con}$	Cross sectional area of HP condenser wall
$A_{wall,eva}$	Cross sectional area of HP evaporator wall
β	PV temperature coefficient
ΔT_{PV}	PV temperature difference
G_{sun}	Solar radiation
h_{conv}	Convective heat transfer coefficient
η_{elec}	Electrical conversion efficiency
η_{ref}	Reference conversion efficiency
I_{bb}	Spectral blackbody emissive power
k_{eff}	Effective thermal conductivity of wick
k_{liq}	Thermal conductivity of HP liquid
k_{sol}	Thermal conductivity of solid wick
k_{wall}	Thermal conductivity of HP wall
L_{RC}	radiative cooler length
$P_{atm,PV}$	Atmospheric radiation absorbed by PV module
$P_{atm,RC}$	Atmospheric radiation absorbed by RC module
$P_{conv,PV}$	Convective heat transfer between PV module and atmosphere
$P_{conv,RC}$	Convective heat transfer between RC module and atmosphere
P_{elec}	Electrical power generated by PV
$P_{rad,PV}$	Radiation emitted from PV module
$P_{rad,RC}$	Radiation emitted from RC module
$P_{sun,PV}$	Solar radiation absorbed by PV
$P_{sun,RC}$	Solar radiation absorbed by RC module
R_{total}	HP total resistance
T_{amb}	Ambient temperature
T_{PV}	Photovoltaic temperature
T_{ref}	Reference temperature
$T_{top,PV}$	Temperature of PV module top side
$T_{top,RC}$	Temperature of RC module top side
v_{wind}	wind speed
δ_{wall}	Thickness of HP wall
δ_{wick}	Thickness of HP wick
ε_{atm}	Atmospheric emissivity
$\varepsilon_{top,PV}$	Emissivity of PV module top side
$\varepsilon_{top,RC}$	Emissivity of RC module top side
Θ	Incident angle
λ	Wavelength

1 Introduction

Over the years, global electricity consumption has risen significantly. Technological, economic, and social factors have influenced this steep rise, and the trend is expected to continue in the future [1]. Particularly, electricity demand for cooling-based applications has escalated [2], and research forecasts that by 2050 the global commercial and residential sectors would undergo a rise in cooling energy demand by 260% and 780%, respectively [3].

There has been a significant progress in electricity generation using solar photovoltaic (PV) technology, as it accounts for the second-largest installed capacity among all renewable energy technologies (25.3% in 2020) [4, 5]. However, as the PV cell operating temperature rises, the power conversion efficiency (or electrical efficiency) decreases linearly due to the intrinsic properties of the materials [6]. Normally, the efficiency of crystalline silicon PV modules decreases at a rate of about 0.35%-0.5% / °C [7]. Simply put, a 100 W rated PV module at standard conditions (25 °C, 1000 W/m^2) would undergo a drop in power output to 87.5-91.5 W when its operating temperature reaches 50 °C. Furthermore, the cell degradation rate doubles for every 10 °C rise in operating temperature [8]. Therefore, PV module cooling is imperative to ensure sufficient power generation and efficiently utilize the available solar energy potential.

When compared to the numerous active PV cooling techniques, the recently introduced radiative cooling (RC) of solar cells has amassed a growing interest among the research community. This is because the RC technique is passive, costs low, and requires little to no structural modifications [9]. By spectrally modifying the radiative properties of the PV module's top side (i.e., facing the sky), the cell temperature can be reduced and PV efficiency improved.

RC to the sky is both energy-efficient and environment-friendly [10] and has been used in diverse applications such as building cooling, renewable energy harvesting, and passive refrigeration [11]. Initially, RC was harnessed only during nighttime because of the high solar gain during the day, but with recent advances in material science, RC can now also be harnessed in the daytime by using novel

materials (e.g., nanoparticle-based [12], photonic-based [10]). Such daytime radiative coolers can significantly reflect solar radiation and simultaneously emit thermal radiation, eventually maintaining a sub-ambient temperature within the presence of sunlight [13, 14]. RC works by radiative heat transfer from high-temperature source (i.e., terrestrial objects at ~300 K) to low-temperature sink (i.e., sky/outer space at ~3 K) [15, 16], in the particular wavelength range from 8-13 μm as the earth's atmosphere is highly transmissive [17-19].

The RC technique for PV module cooling was first investigated by Zhu et al. [20, 21], who designed a silica photonic radiator which reduced the cell temperature by 17.6 °C (for pyramid-shaped) and 12.4 °C (for planar-shaped), compared to a bare silicon solar cells which have negligible RC ability. RC in nanowire-shaped GaAs solar cells were simulated by Wu and Povinelli [22], who reported a 7 °C temperature drop compared to the conventional planar-shaped cells. Another radiative cooler was proposed by Safi and Munday [23], which improved the cell efficiency by 0.87% compared to a cell with no RC. Similarly, many other studies have reported considerable solar cell temperature reduction using the RC technique [24-26].

However, the results mentioned in the abovementioned studies are mainly over predicted, since the PV temperature reduction from RC was compared to that with bare solar cells instead of the conventional glass encapsulated solar cells. Usually, solar cells are encapsulated with glass, which has a relatively high thermal emissivity (ε = 0.8-0.90 [27, 28]) and possesses an inherent RC ability. Thus, with the highly emissive ideal radiators (ε = ~1) placed on top, the cell temperature reduction would not be substantially high compared to glass encapsulated cells. Considering this issue, some studies [29-31] investigated the comparative performance between solar cells with ideal radiators and those with glass covers and found the highest difference in temperature reduction between the two cases to be around 1 °C. Li et al. [32] also conducted outdoor field tests and experimentally verified the insignificant temperature reduction. Recently, Ahmed et al. [33] investigated the comparison between glass and ideal RC on a photovoltaic-thermal system and found that a mere 0.5% efficiency improvement was possible.

Therefore, spectrally modifying the existing PV module covers or substituting them with novel RC materials is not an efficient technique for passive PV cooling. In order to maximize the RC potential to the sky and to significantly reduce the PV temperature, a new PV system configuration needs to be designed, with three primary requirements. Firstly, the RC module should not replace the existing PV glass encapsulation so that the natural RC ability of glass can be harnessed and add to the overall cooling gain. Secondly, the RC module should directly face the sky (i.e., largest view factor) to radiate maximum waste heat into outer space. Thirdly, there should be an efficient and quick heat transfer mechanism between the PV (i.e., heat source) and RC (i.e., heat sink) modules.

In response to the abovementioned requirements, this study proposes a system that consists of a PV module and a separate RC module, integrated with a heat pipe (HP) in between (**Fig. 1**). HPs are passive heat transfer devices with different configurations and used in diverse application areas including solar water heating [34], solar cooking [35], waste heat recovery [36] etc. The first requirement is satisfied by using a separate RC module alongside the pre-existing glass cover. For the third condition, a HP is integrated between the two modules. The second condition is also supported by using a HP since the RC module is placed on its condensing section and faces the sky. The PV module is placed on the evaporating section, and waste heat from the cells is radiated out simultaneously from both the RC module and the glass cover. As a result, a significant reduction in solar cell operating temperature and a rise in electrical efficiency are obtained. Although PV cooling using HPs has been investigated before, the previous condensers were cooled using techniques like low ambient temperature [37], metallic fins [38, 39], thermoelectric generator [40], and water flow [41, 42]. This is the first study that investigates the technique of radiative emission to the cold sky for cooling the HP condenser and eventually reducing the PV module temperature.

First, the numerical models were developed using COMSOL Multiphysics 5.5 and then validated with the literature. In order to investigate the proposed system's performance, the models were comparatively analyzed against other similar systems from the literature. The effects of varying different input parameters on the system performance were also investigated in order to design a

system suitable for various operating conditions. Detailed descriptions of the proposed system's working principle, configuration, and properties are presented in section 2. Alternate systems that were considered to comparatively analyze the performance are also detailed. Section 3 explains the numerical modeling of each subsystem (PV, HP, RC) and the combined system. Section 4 presents the results and their corresponding discussion, while section 5 gives the conclusions.

2 System description

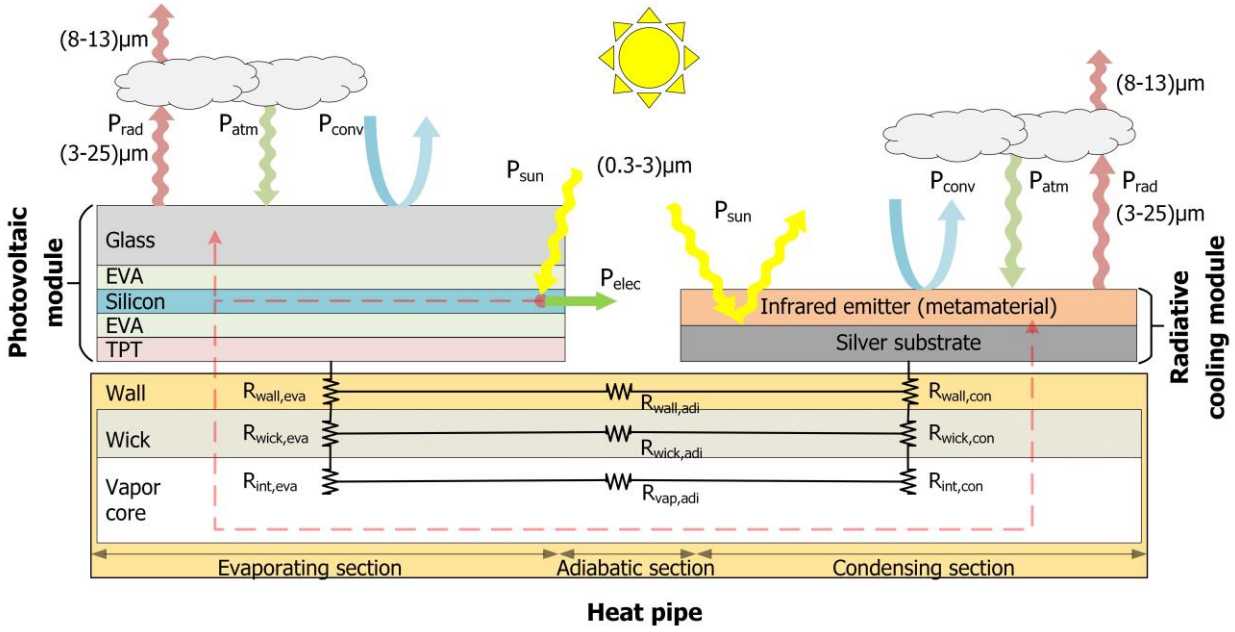

Fig. 1. Schematic of the operating principle, configuration, and boundary conditions of the proposed PV-HP-RC system

2.1 Operating principle

As shown in **Fig. 1,** the proposed system consists of a PV module placed on the evaporating section of the HP, while an RC module is placed on the condensing section, each module facing the sky. During the day, solar radiation reaches the silicon layer (P_{sun}) after transmission through the above layers and gets partially converted into electricity (P_{elec}). The remaining solar energy (P_{sun} - P_{elec}) is the waste heat, and a part of it is lost from the top side of the PV module through radiation (P_{rad}) and convection (P_{conv}), while another part of it gets transferred to the HP via conduction between the layers. Within the HP, the heat is transferred from its evaporating section to the condensing section via a phase change process explained later. At the condensing section, the heat is released from the

top surface of the RC module via radiation to the sky (P_{rad}) and convection with the atmosphere (P_{conv}).

The idea for this research was inspired by the work of Ezekwe [43], who designed a refrigerator using the RC technique integrated with HP. However, in that period, RC could only be harnessed during nighttime. With the recent emergence of advanced materials and fabrication techniques, RC can now be harnessed in the daytime within the presence of sunlight since the radiative coolers can simultaneously reflect solar radiation and emit thermal radiation. The major novelty for this study is the use of such daytime radiative coolers on the condensing section of the HP in order to reduce the solar cell operating temperature. In conclusion, the efficiency of the PV system is improved as the waste heat from the cells is released from both the top of the PV module and the RC module, while the HP serves as a heat transfer mechanism between the two. The individual module configurations, properties, and working principles are explained in the following section.

2.2 Configuration and properties

A typical solar PV module consists of five layers: glass, ethyl vinyl acetate (EVA), Si solar cells, EVA, and tedlar polyester tedlar (TPT). Glass provides mechanical strength and high transmission of solar radiation. EVA is an encapsulant and provides adhesions between the different layers. The solar cells convert solar radiation into electricity via the photovoltaic effect, while TPT protects the back surface.

HP is a passive heat transfer device consisting of a tube with a porous wick lined on the inner wall surface and a vapor core in the center (**Fig. 1**). Initially, the wick of the HP contains liquid at a saturated state, while the core contains some vapor. When waste heat from the PV module moves via conduction to the evaporating section of the HP, the saturated liquid in that section vaporizes, causing the vapor pressure to rise. This difference in vapor pressure drives the vapor through the core of the HP from the evaporating section to the condensing section. Since the condensing section of HP is kept in a slightly cooler environment (i.e., due to solar reflection), the vapor there condenses to liquid,

releasing its heat of vaporization, which is released to outer space through thermal radiation. The liquid returns to the evaporating section through the porous wick through capillary action, and the cycle continues. The adiabatic section in between is where the vapor and liquid move in opposite directions. This study considered a flat HP rather than a cylindrical HP for maximum heat transfer area between the PV module backside and the evaporating section, and also between the RC module backside and the condensing section. Note that the HP is considered insulated on its bottom side, while heat transfer occurs on the top side since we are only interested in RC to the sky. Also, since the module is expected to be installed on a building's roof, heat transfer from the HP bottom side would require an additional cooling mechanism and is therefore assumed to be insulated. As detailed in section 3.3, the thermal resistance network approach was used to model the HP since it is straightforward, computationally efficient, and reasonably accurate.

To achieve daytime RC, the materials used in the RC module should have two main properties. Firstly, it should be highly reflective in the short solar wavelengths (0.3-3 μm) to reflect the radiative heat from the sun. Secondly, it should be highly emissive in the longer wavelengths (3-25 μm) to radiate maximum heat from itself. Since solar cells operate at much higher temperatures than the ambient temperature, for the proposed system, a broadband radiator (i.e., highly emissive in 3-25 μm) is preferred in contrast to a narrow band radiator (i.e., highly emissive in 8-13 μm), as the RC module also operates at above ambient temperatures [19, 44]. The RC module consists of two layers, with the bottom layer being a silver film for reflection of incident solar radiation. For radiative emission from the top layer, different materials were investigated in the literature (i.e., nanophotonics [21], metamaterials [45], etc.). For this study, we considered an ideally emissive material, that has a unity emissivity ($\varepsilon = 1$) in the longer wavelengths, similar to the glass-polymer hybrid metamaterial in Ref [45] . The geometric and material properties used in this study are reported in **Table 1**.

Table 1. Geometric and material properties used in the numerical simulation [15, 40].

Sub-system	Material	Length (m) x Width (m)	Thickness (mm)	Thermal conductivity (W/mK)

PV module		1 × 1		
Layer 1	Glass		3.2	2
Layer 2 and 4	EVA		0.46	0.3
Layer 3	Silicon		0.18	130
Layer 5	TPT		0.18	0.15
HP				
Evaporating section		1 × 1		
Condensing section		1 × 1		
Wall	Copper		5	400
Wick	Copper (wrapped screen)		5	1.823
Fluid	Water			0.61
RC module		1 × 1		
Solar reflector	Silver film		1×10^{-3}	429
IR emitter	Ideal emitter		1	

2.3 Cases investigated

Since our proposed system consists of a PV module, HP, and RC module, hereafter, it is referred to as the PV-HP-RC system. To evaluate the performance of the PV-HP-RC system, two other types of systems from the literature were compared. First was the base case, which consists of a PV module with a conventional glass cover on top [46]. The usual convective and radiative heat loss from the top side and convective loss from the bottom side is expected without considering any additional cooling. This case is referred to as the PV-Glass case. For the second case, the regular glass cover was replaced with an ideally emissive radiative cooler on top of the solar cells, as in Ref. [32]. The only difference between these two cases is that with the ideal radiative cooler on top, the RC ability is enhanced because glass has a relatively lower emissivity than the novel RC materials. This case is referred to as the PV-RC case. The third case is the proposed PV-HP-RC case which has been detailed in section 2.1. **Fig. 2** shows a schematic of the cases investigated, and **Table 2** gives the values for the optical properties used in the simulation.

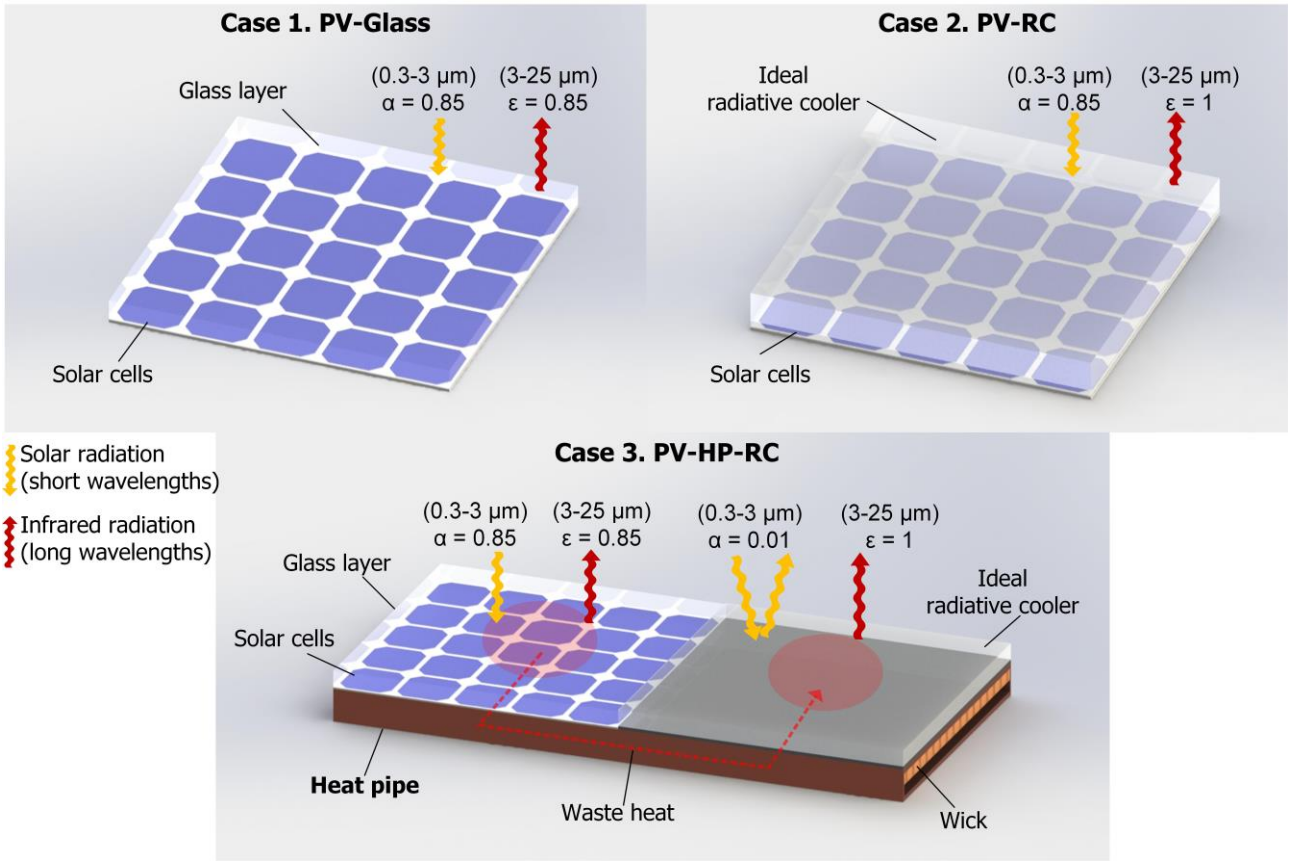

Fig. 2. Schematic of the different cases simulated to compare the proposed system's performance.

Table 2. Optical properties used in the simulation [15, 33].

Case	PV top (absorptivity/emissivity)		RC top (absorptivity / emissivity)	
	(0.3-3 μm)	(3-25 μm)	(0.3-3 μm)	(3-25 μm)
1. (PV-Glass)	0.9	0.85	-	-
2. (PV-RC)	0.9	1	-	-
3. (PV-HP-RC)	0.9	0.85	0.01	1
	Atmospheric emissivity			
	(0.3-3 μm)	(3-8 μm)	(8-13 μm)	(13-25 μm)
	0.9	0.9	0.2	1

3 Numerical modeling

In this section, we describe the numerical model developed for the proposed system. At first, individual thermal models for the PV module, RC module, and the HP were developed and then integrated into a hybrid system to simulate the aforementioned cases.

The 1D steady-state heat diffusion equation used for the modeling is shown as:

$$k\frac{\partial^2 T}{\partial z^2}+q=0 \tag{1}$$

where T is the temperature distribution in the vertical direction (z), K; k is thermal conductivity, W/(mK); and q is internal heat generation, W/m^2.

3.1 Photovoltaic module

The following assumptions were considered to simplify the model with minimum deviation from the real case [40, 47]:

- All layers have equivalent cross-sectional areas and are in direct contact.
- The thermal properties of all materials are constant and isotropic.
- Convective heat transfer with atmosphere and radiative heat transfer with the sky is considered on the top side, while only convective heat transfer is considered on the bottom side.
- The convective heat transfer coefficient on the top and bottom sides is considered equivalent.
- Absorptivity and emissivity are considered directionally independent.

The heat source is the waste heat generated in the Si layer, which is the difference between the absorbed solar power and generated electrical power given as:

$$q = P_{sun,PV} - P_{elec} \tag{2}$$

where $P_{sun,PV}$ is the solar radiation absorbed by the Si layer, W/m^2; and P_{elec} is electrical power generated W/m^2.

$$P_{sun,PV} = \tau\alpha \cdot G_{sun} \tag{3}$$

where $\tau\alpha$ is the transmittance-absorptance product and gives the fraction of solar radiation that reaches the Si layer ($\tau\alpha$ = 0.9 [48]); and G_{sun} is the solar radiation incident on the topmost layer of PV module, W/m^2.

$$P_{elec} = \eta_{elec} \cdot P_{sun,PV} \tag{4}$$

where η_{elec} is the electrical conversion efficiency of the PV module and is calculated as:

$$\eta_{elec} = \eta_{ref}[1-\beta(T_{PV} - T_{ref})] \tag{5}$$

where η_{ref} is the reference conversion efficiency (η_{ref} = 0.2); β is temperature coefficient of crystalline Si cells (β = 0.0045 K^{-1}); T_{PV} is the PV operating temperature which is the average temperature of the Si layer, K; and T_{ref} is the reference temperature (T_{ref} = 298.15 K). Note that η_{elec} linearly decreases with rise in $T_{PV.}$

The following boundary condition is used for the top side of the PV module:

$$k\frac{\partial T}{\partial z}_{top,PV} = P_{rad,PV} - P_{atm,PV} + P_{conv,PV} \tag{6}$$

where $P_{rad,PV}$ is radiation emitted by PV top surface, W/m^2; $P_{atm,PV}$ is radiation absorbed by PV top surface that is emitted from the atmosphere; and $P_{conv,top}$ is convective heat transfer between PV top surface and atmosphere, and are evaluated as follows [19]:

$$P_{rad,PV} = 2\pi\int_0^{\frac{\pi}{2}}\int_0^{\infty}\varepsilon_{top,PV}(\theta,\lambda)I_{bb}(\lambda,T_{top,PV})\sin(\theta)\cos(\theta)d\lambda d\theta \tag{7}$$

where $\varepsilon_{top,PV}$ is the spectral directional emissivity of PV top surface; I_{bb} is the spectral radiance of blackbody at $T_{top,PV}$ and is evaluated as:

$$I_{bb}(\lambda,T_{top,PV}) = \frac{2hc_0^2}{\lambda^5\left\{\exp\left[hc_0/\left(\lambda k_B T_{top,PV}\right)\right]-1\right\}} \tag{8}$$

where h is the Planck constant (h = 6.626×10^{-34} J·s); k_b is the Boltzmann constant (k_b = 1.381×10^{-23} J/K); and c_0 is the speed of light (c_0 = 3×10^{-8} m/s).

$$P_{atm,PV} = 2\pi \int_0^{\frac{\pi}{2}} \int_0^{\infty} \alpha_{top,PV}(\theta,\lambda)\varepsilon_{atm}(\theta,\lambda)I_{bb}(\lambda,T_{amb})\sin(\theta)\cos(\theta)d\lambda d\theta \quad (9)$$

where $\alpha_{top,PV}$ is absorptivity of PV top surface and is equivalent to the emissivity according to Kirchhoff's radiation law [15]; ε_{atm} is the emissivity of the atmosphere mainly from water vapor and carbon dioxide molecules; T_{amb} is the ambient temperature.

$$P_{conv,PV} = h_{conv}(T_{top,PV} - T_{amb}) \quad (10)$$

where h_{conv} is the convective heat transfer coefficient and is evaluated as:

$$h_{conv} = 2.8 + 3v_{wind} \quad (11)$$

where v_{wind} is the atmospheric wind speed, m/s. Note that numerous relations for h_{conv} have been reported in the literature, and the one used here is taken from [48]

The boundary condition used for the bottom side of the PV module is given as:

$$k\frac{\partial T}{\partial z}_{btm,PV} = P_{conv,btm} = h_{conv}(T_{btm,PV} - T_{amb}) \quad (12)$$

By applying the boundary conditions on the heat diffusion equation, T_{PV} is evaluated and will be discussed in section 4.

3.2 Radiative cooling module

The following boundary condition is used for the top side of the RC module:

$$k\frac{\partial T}{\partial z}_{top,RC} = \mathrm{P}_{rad,RC} - P_{sun,RC} - P_{atm,PV} + P_{conv,RC} \quad (13)$$

where $P_{rad,RC}$ is radiation emitted by top surface of RC module, W/m^2; $P_{sun,RC}$ is radiation absorbed by top surface emitted from the sun, W/m^2; $P_{atm,RC}$ is radiation absorbed by top surface emitted from the atmosphere, W/m^2; $P_{conv,top}$ is convective heat transfer between PV top surface and atmosphere, W/m^2, and are evaluated as follows [19]:

$$P_{rad,RC} = 2\pi \int_0^{\frac{\pi}{2}} \int_0^{\infty} \varepsilon_{top,RC}(\theta,\lambda) I_{bb}(\lambda, T_{top,RC}) \sin(\theta)\cos(\theta) d\lambda d\theta \tag{14}$$

$$P_{sun,RC} = 2\pi \int_0^{\frac{\pi}{2}} \int_0^{\infty} \alpha_{top,RC}(\theta,\lambda) \varepsilon_{top,RC}(\theta,\lambda) I_{bb}(\lambda, T_{sun}) \sin(\theta)\cos(\theta) d\lambda d\theta \tag{15}$$

$$P_{atm,RC} = 2\pi \int_0^{\frac{\pi}{2}} \int_0^{\infty} \alpha_{top,RC}(\theta,\lambda) \varepsilon_{atm}(\theta,\lambda) I_{bb}(\lambda, T_{amb}) \sin(\theta)\cos(\theta) d\lambda d\theta \tag{16}$$

$$P_{conv,RC} = h_{conv}(T_{top,RC} - T_{amb}) \tag{17}$$

The boundary condition used for the bottom side of the RC module is given as:

$$k \frac{\partial T}{\partial z}_{btm,RC} = P_{conv,btm} = h_{conv}(T_{btm,RC} - T_{amb}) \tag{18}$$

3.3 Heat pipe

The liquid to vapor (in evaporating section) and vapor to liquid (in condensing section) phase change process inside the HP, for a desired operating temperature, takes place at the saturation pressure for the particular working fluid. In this study, we have not designed a HP from start, and thus the operating temperature and pressure have not been considered. Instead, the use of a HP as a device to transport heat has been considered assuming that a steady phase change process takes place. The thermal resistance network approach is a useful technique to model steady-state heat transfer problems in simple geometries and therefore has been used to model the HP. **Fig. 1** presented the thermal resistances for a typical flat plate HP, which are detailed in **Table 3**.

Table 3. Thermal resistances used for modeling the heat pipe [49, 50].

Resistance	Description
$R_{wall,eva}$	Resistance of wall in evaporating section
$R_{wall,con}$	Resistance of wall in condensing section
$R_{wick,eva}$	Resistance of liquid-wick combination in evaporating section
$R_{wick,con}$	Resistance of liquid-wick combination in condensing section
$R_{wall,adi}$	Resistance of wall in adiabatic section
$R_{wick,adi}$	Resistance of wick in adiabatic section
$R_{vap,adi}$	Resistance of vapor pressure drop in adiabatic section
$R_{int,eva}$	Resistance of liquid-vapor interface evaporating section
$R_{int,con}$	Resistance of liquid-vapor interface condensing section

By using the electrical circuit analogy, parallel resistance that have large values (i.e., $R_{wall,adi}$ and $R_{wick,adi}$) can be considered as open circuit and are omitted. Series resistances with small values (i.e., $R_{vap,adi}$, $R_{int,eva}$ and $R_{int,con}$) can be considered as a short circuit and are also neglected [49]. Also, note that the thermal contacts between the heat source with evaporating section and the heat sink with condensing section are assumed to be ideal, and therefore the thermal contact resistance is considered negligible. This can be achieved by using thermal grease as the interface between different components. Total thermal resistance for the heat pipe is calculated as:

$$R_{total} = R_{wall,eva} + R_{wick,eva} + R_{wick,con} + R_{wall,con} \tag{19}$$

where $R_{wall,eva}$ and $R_{wick,eva}$ are evaluated as:

$$R_{wall,eva} = \frac{\delta_{wall}}{k_{wall} A_{wall,eva}} \tag{20}$$

where δ_{wall} is wall thickness, k_{wall} is wall thermal conductivity, and $A_{wall,eva}$ is the cross-sectional area of wall in evaporating section area

$$R_{wick,eva} = \frac{\delta_{wick}}{k_{eff} A_{wick,eva}} \tag{21}$$

where δ_{wick} is the wick thickness, $A_{wick,eva}$ is the cross-sectional area of wick in evaporating section, and k_{eff} is thermal conductivity of liquid saturated wick evaluated as

$$k_{eff} = \frac{k_{liq}[(k_{liq} + k_{sol}) - (1-\varepsilon)\cdot(k_{liq} - k_{sol})]}{(k_{liq} + k_{sol}) + (1-\varepsilon)\cdot(k_{liq} - k_{sol})} \quad (22)$$

where k_{liq} is the thermal conductivity of HP fluid (water), k_{sol} is the thermal conductivity of the solid wick (copper); and ε is the wick porosity (ε = 0.5). This relation for k_{eff} is for a wrapped screen wick structure, while relations for other structures can be found in Ref. [49]. $R_{wall,con}$ and $R_{wick,con}$ are evaluated similarly using corresponding values for the condensing section.

3.4 Hybrid model

The numerical simulations were performed in COMSOL Multiphysics 5.5 software. The heat-transfer-in-solids and surface-to-surface-radiation interfaces were used to model the boundary conditions used in the PV module and RC module. The lumped-thermal-system interface was used to model the thermal resistance network for the HP. Once the individual model for each subsystem was developed and validated, they were then connected by using the lumped system connector and external terminal nodes in the heat-transfer-in-solids and lumped-thermal-system interface, respectively. Atmospheric data, including solar radiation (G_{sun}), ambient temperature (T_{amb}), and wind speed (v_{wind}), was used as input boundary conditions and was updated for every one-hour time interval. Modeling steps are available by following the software guide [51] and similar models available in the application gallery [52].

3.5 Model validation

In order to validate the numerical models developed in this study, a comparison was made with similar models in the literature. The model for the PV module presented in [31] was used to validate the PV model of this study. Similar operating conditions were used for an accurate comparison. The PV temperature variation against the changing solar radiation was compared (**Fig. 3a**). As for the RC module, the model presented in [53] was used for validation. The radiative cooling power of the module was investigated by varying the temperature of the top surface (**Fig. 3b**). Lastly, the heat pipe model was validated in COMSOL using the data from a similar example problem in Ref. [49]. The

results are not presented here since the input parameter was not varied and only a single output value was checked.

The average differences between the previous and present studies were 0.5 °C for PV temperature and 3.4 W/m^2 for radiative cooling power, both of which are insignificant. Therefore, it shows that the models developed in this study were very similar to those presented in previous studies. This confirms that the results obtained hereafter are accurate and justifiable. It should be noted that our model validation approach follows the one used in Ref. [40] which developed a similar hybrid model of a PV-HP-thermoelectric system.

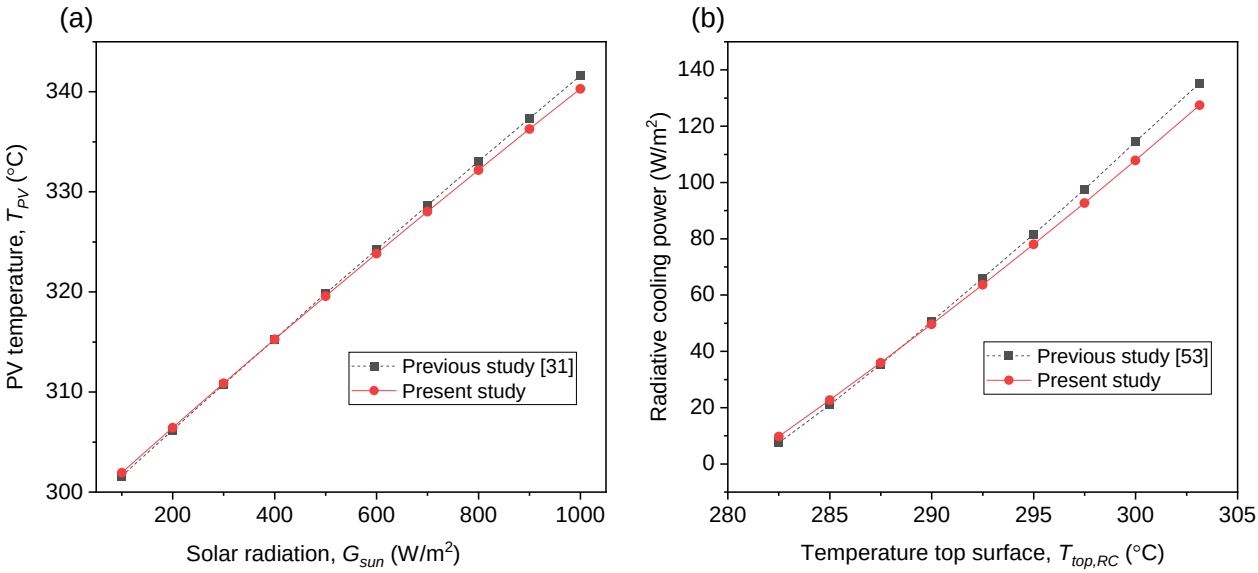

Fig. 3. Model validation of present study with previous studies by comparing (a) PV temperature for the PV model and (b) radiative cooling power for the RC model.

4 Results and discussion

In this section, the results obtained for the daytime working performance of each case are compared. Furthermore, a parametric analysis was done to investigate the effects of different factors on system performance.

4.1 Performance evaluation

Atmospheric data (i.e., solar radiation, ambient temperature, wind speed) for the city of Las Vegas was used as input as boundary conditions for the numerical models. This is because the city experiences high solar radiation, which is appropriate for PV power generation, and low humidity, which is suitable for RC. **Fig. 4** shows the weather data taken from EnergyPlus software [54] for a regular summer day in June during the daytime operating period (9:00-16:00).

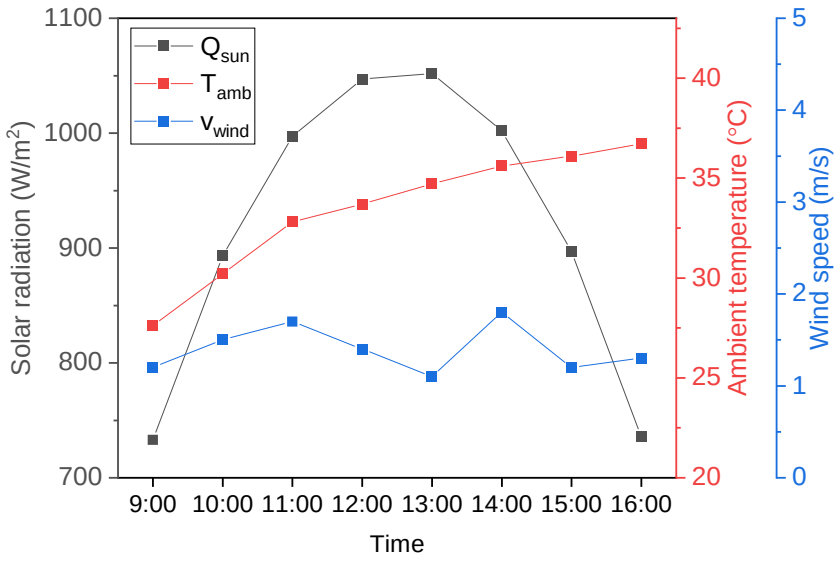

Fig. 4. Atmospheric data used as input boundary conditions in the simulation

The ultimate goal of the proposed system is to reduce the operating temperature of the solar cells so to improve their electrical efficiency, as detailed in Eq. (5). Therefore, the variation in PV operating temperature (T_{PV}) and corresponding electrical conversion efficiency (η_{elec}) for each case was simulated for every hour and as is represented in **Fig. 5**. PV-HP-RC shows the lowest T_{PV} and highest η_{elec} amongst all cases throughout the day and is followed by PV-RC and PV-Glass cases. The highest reduction in T_{PV} between PV-Glass (i.e., conventional system) and PV-HP-RC (i.e., proposed system) occurs at 13:00, which is 12.86 °C and corresponds to a relative rise in η_{elec} of 7.25%.

The significant temperature reduction using PV-HP-RC supports the effectiveness of the proposed system. RC of solar cells using a PV-HP-RC system is considerably more useful than the previously investigated PV-RC systems. It is evidenced by the average reduction in T_{PV} from PV-RC, which is

around 2 °C (**Fig. 5**), as was also reported by Ref. [31] and Ref. [32]. Despite the relatively large temperature reduction, it can be argued that PV-HP-RC requires twice the area as a PV-RC system. This issue can be addressed by using the additional area to harness nighttime cooling, as was studied by Ref. [53].

A PV-HP-RC system has the most suitable configuration to maximize the radiative heat loss to the sky. This is because heat is radiated from both the PV module topside (i.e., glass cover) as well as the RC module topside. In contrast, for the PV-Glass and PV-RC cases, heat will only be radiated out from the PV module topside, and thus the cell temperature remains high.

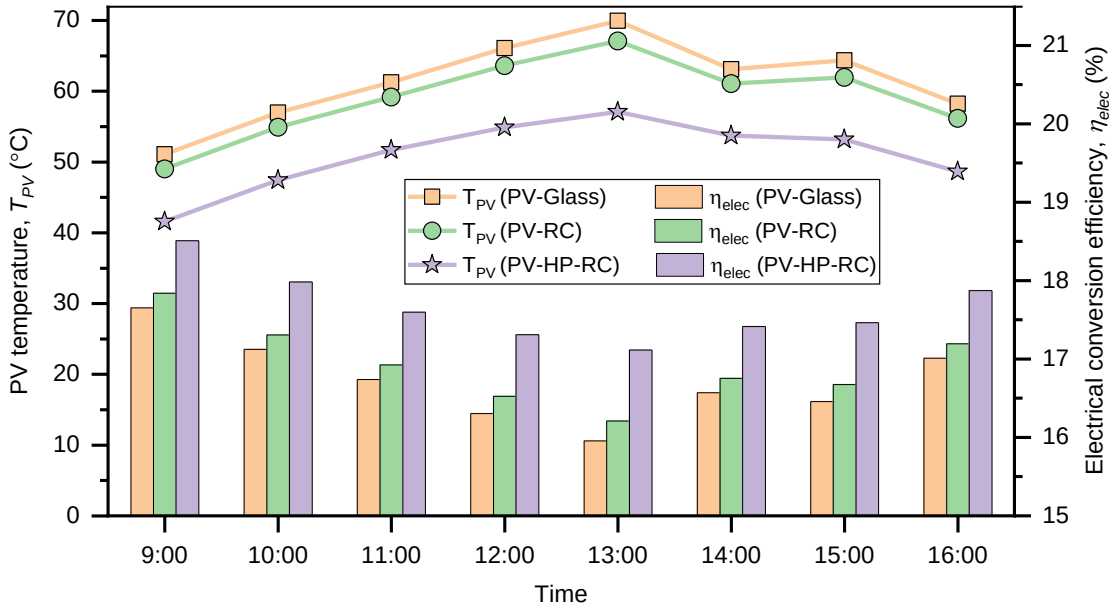

Fig. 5. Photovoltaic temperature and electrical conversion efficiency for each case simulated

4.2 Parametric analysis

There are many input parameters that influence the cooling performance of the proposed PV-HP-RC system. In this section, we conducted a parametric analysis to analyze the impact of external parameters like solar radiation (G_{sun}), ambient temperature (T_{amb}), wind speed (v_{wind}), atmospheric emissivity (ε_{amb}), and internal parameters such as RC module length (L_{RC}), and HP resistance (R_{total}). The values for the parameters considered in the base case are given in **Table 4**.

Table 4. Operating parameters considered for base case

Parameter	Value
Solar radiation	1000 W/m^2
Ambient temperature	30 °C
Wind speed	1 m/s
Atmospheric emissivity	0.2
Radiative cooler length	1 m
HP resistance	0.005 °C/W

In response to these varying input parameters, the system performance was evaluated using two output indicators: 1. PV operating temperature (T_{PV}) as given in Eq. (5), and 2. difference in PV temperature (ΔT_{PV}) between the PV-Glass (i.e., conventional case) and PV-HP-RC (i.e., proposed case) using Eq. (23):

$$\Delta T_{PV} = T_{PV(PV-Glass)} - T_{PV(PV-HP-RC)} \tag{23}$$

ΔT_{PV} is a useful indicator to compare the temperature difference between the conventional and proposed cases. A higher value for ΔT_{PV} indicates the usefulness of the PV-HP-RC system.

Since the RC module at the condenser section is open to the atmosphere, it releases the heat by radiation to the sky as well as convection to the ambient air. Therefore, the share of each heat transfer mechanism is also investigated by considering two other output indicators: 1. net radiative cooling power ($P_{net,RC}$) using Eq. (24), and 2. convective cooling power ($P_{conv,RC}$) as given in Eq. (17).

$$P_{net,RC} = \mathrm{P}_{rad,RC} - P_{sun,RC} - P_{atm,RC} \tag{24}$$

4.2.1 Solar radiation

When solar radiation (G_{sun}) rises, T_{PV} increases from 28.04 to 59.98 ℃, due to the increased solar heat absorption (**Fig. 6**). ΔT_{PV} increases from 6.31 to 14.89 ℃, since more waste heat is lost from the top sides of PV and RC modules. Since the PV-HP-RC system shows improved performance at higher G_{sun}, therefore it should be installed in locations that experience high solar gain throughout the year. $P_{net,RC}$ rises from 109 to 293.75 W/m^2, since larger G_{sun} means more heat is being transferred through the HP to the RC panel and eventually emitted as radiation. $P_{conv,RC}$ rises from -15.82 to 152.54 W/m^2, due to the higher RC panel temperature. Note that at G_{sun} = 250 W/m^2, $P_{conv,RC}$ is -15.82 W/m^2, which

indicates that at such lower G_{sun}, the atmosphere contributes to convective heat gain rather than a heat loss, and is because the temperature of RC panel is below T_{amb}.

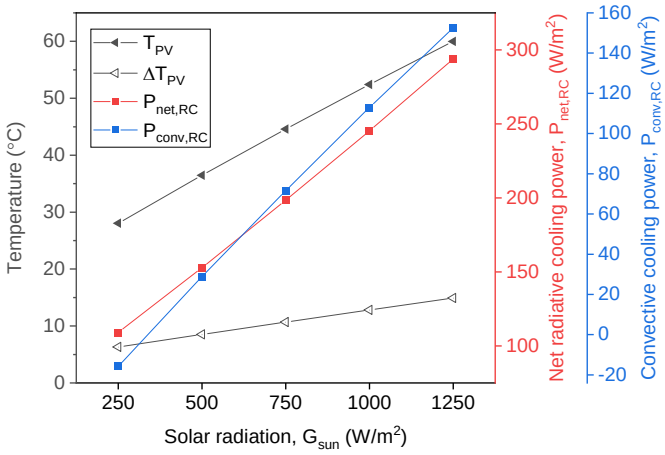

Fig. 6. Variation in system output indicators with solar radiation.

4.2.2 Ambient temperature

The rise in ambient temperature (T_{amb}) increases the radiative heat gain from the atmosphere on both the PV module top side [$P_{atm,PV}$ in Eq. (9)] and RC module top side [$P_{atm,RC}$ in Eq. (16)]. Furthermore, convective cooling power from both modules also reduces since the difference in temperature between the top and ambient temperature has been reduced, and is evident from **Fig. 7**, where $P_{conv,RC}$, shows a decreasing trend. Eventually, T_{PV} increases linearly from 44.88 to 59.94 °C. $\Delta T_{PV,}$ on the other hand, remains almost constant, and this is because, in the PV-HP-RC system, the RC module does not reflect any ambient radiation since it is within the MIR band, for which the top side has high absorptivity/emissivity.

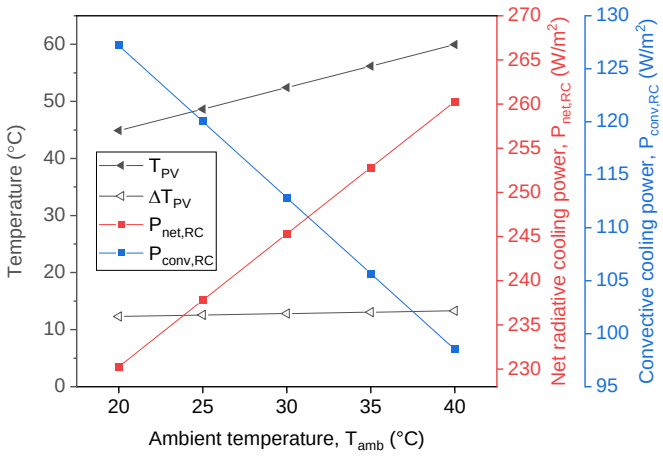

Fig. 7. Variation in system output indicators with ambient temperature.

4.2.3 Wind speed

The wind speed (v_{wind}) is related to the convective heat transfer coefficient using Eq. (11). An increase in $v_{wind,}$ enhances the convective heat transfer from both the PV top side and RC top side, eventually reducing the T_{PV}. **Fig. 8** shows that as v_{wind} increases from 0 to 4 m/s, T_{PV} decreases from 58.48 to 43.90 °C. Note that ΔT_{PV} reduces from 22.04 to 4.40 °C, signifying that the T_{PV} reduction potential from the PV-HP-RC system reduces at higher v_{wind} since convective cooling becomes dominant over RC. This is justified since $P_{net,RC}$ and $P_{conv,RC}$ have an inverse relationship with each other. Thus, the proposed PV-HP-RC system should be installed in areas where v_{wind} remains considerably low so to maximize the RC ability. The increase in v_{wind}, causes $P_{conv,RC}$ to increase from 71.33 to 163.38 W/m^2, while $P_{net,RC}$ reduces from 292.4 to 183.72 W/m^2.

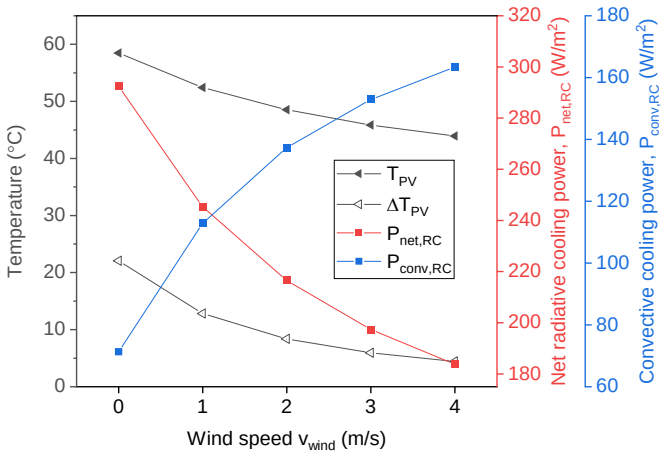

Fig. 8. Variation in system output indicators with wind speed

4.2.4 Atmospheric emissivity

The relative humidity corresponds to the presence of water vapor in the atmosphere, and is therefore related to the atmospheric emissivity (ε_{atm}) [19]. A higher ε_{atm} means there are more water vapor molecules and thus more atmospheric radiation incidents on the PV and RC module. We investigated the impact of varying ε_{atm}, particularly within the 8-13 μm range since this is where the atmosphere has the highest transmissivity (i.e., least emissivity). As ε_{atm} increases from 0.1 to 0.5, so does the atmospheric radiation incident on the RC module [$P_{atm,RC}$ in Eq.(16)], and therefore $P_{net,RC}$ reduces (**Fig. 9**). Correspondingly $P_{conv,RC}$ increases in order to maintain energy conservation. Note that the changes in radiative and convective cooling power are not large (~30 W/m^2), and thus T_{PV} shows a very small rise from 51.27 to 55.7 °C. It can be concluded that changes in ε_{atm} will not have a significant effect on the performance of the proposed system.

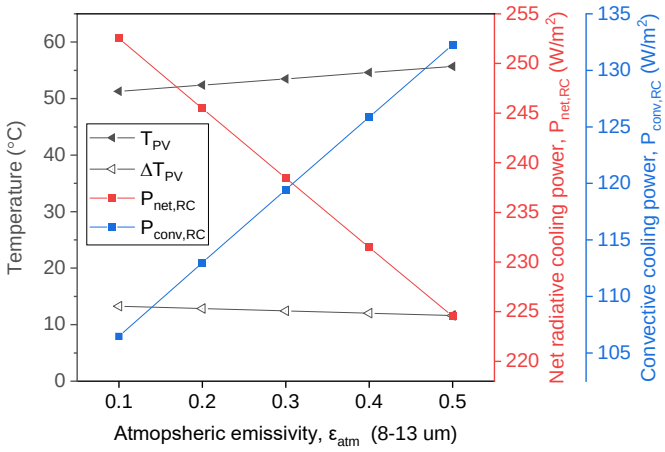

Fig. 9. Variation in system output indicators with atmospheric emissivity.

4.2.5 Radiative cooler length

The impact of internal design parameters were also investiaged in addition to the external atmospheric parameters (G_{sun}, T_{amb}, v_{wind}, ε_{atm}) as discussed above. The length of the RC module (L_{CR}) corresponds to the area of the HP condensing section. Increasing L_{RC}, means more heat can be released out from the RC module through radiation ($P_{rad,RC}$) and convection ($P_{conv,RC}$), but the amount of atmospheric radiation ($P_{atm,RC}$) absorbed by the module would also increase. However, since the released heat is considerably large compared to the absorbed radiation, T_{PV} shows a decreasing trend from 61.73 to 46.83 C, when L_{RC} is increased from 0.5 to 1.5 m (**Fig. 10**). Note that ΔT_{PV} is not represented since L_{RC} is not an available parameter in PV-Glass case.

$P_{net,RC}$ and $P_{conv,RC}$ show a decreasing trend, and this is because the graph does not show the absolute magnitude of the heat (W) but instead the heat flux (W/m^2); even though the flux is decreasing, the total magnitude of heat released increases. The larger the $L_{RC,}$ the better would be the system performance in reducing PV temperature, but this depends on design constraints (i.e., HP limiting condition [49]) and economic feasibility.

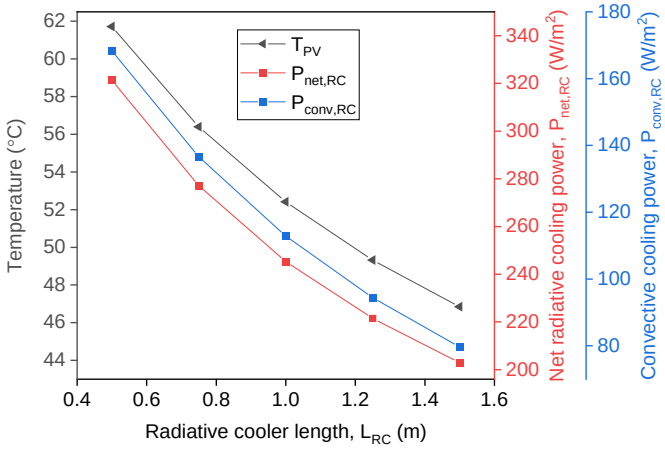

Fig. 10. Variation in system output indicators with radiative cooler length.

4.2.6 Heat pipe resistance

As discussed in section 3.3, the total thermal resistance of the HP (R_{total}) is dependent on a number of geometrical and material properties. These include the thickness, thermal conductivity, and cross-sectional area of the HP wall, wick, and liquid. The combined effect of these properties gives R_{total} [from Eq. (19)], and its effect on the system performance was investigated. Increasing R_{total} drastically increases T_{PV} from 51.57 to 76.73 °C, as shown in **Fig. 11**. It is because heat transfer from the evaporator (i.e., PV module backside) to the condenser (i.e., RC module backside) reduces with the rise in thermal resistance, and the waste heat from the solar cells gets accumulated, eventually raising T_{PV}. Correspondingly, $P_{net,RC}$ undergoes a significant reduction since the temperature of the RC panel [$T_{top,RC}$ in Eq. (14)] is also reduced. $P_{conv,RC}$ also decreases because the temperature difference between RC panel and ambient has diminished. A PV-HP-RC system effectively reduces the PV temperature only if the different thermal resistances associated with a HP are kept as low as possible. Thus, thoughtful consideration must be undertaken while deciding the HP material and geometric properties.

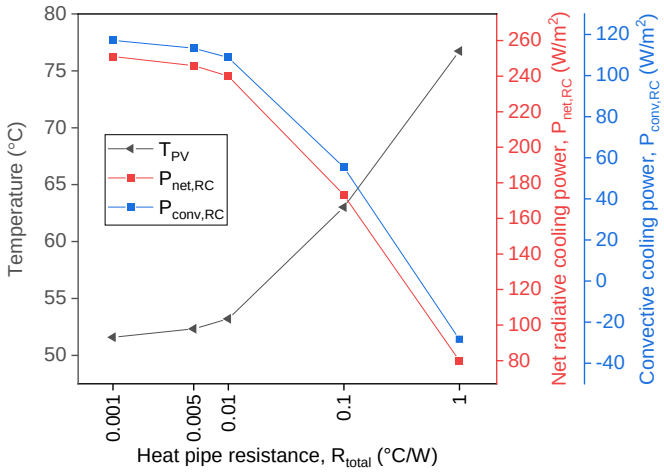

Fig. 11. Variation in system output indicators with heat pipe resistance.

5 Conclusions

In this study, we investigated a novel system configuration for enhanced cooling of solar cells by integrating a photovoltaic (PV) module and a radiative cooling (RC) module with a heat pipe (HP) in between. A thermal model for the proposed system was first developed and then numerical simulations were conducted to evaluate the system performance. Two other cases from the literature were modeled and simulated under similar operating conditions to compare the performance of the proposed system. Furthermore, varying the external and internal input parameters and their effects on performance indicators was studied. The significant findings from this study show that:

- The highest reduction in solar cell operating temperature between the PV-Glass case (i.e., conventional system) and PV-HP-RC case (i.e., proposed system) is 12.86 °C, which corresponds to a relative rise in the electrical efficiency of 7.25%, and indicates the usefulness of the proposed system.
- Different input parameters have varying effects on the system performance. Compared to the conventional system, the usefulness of the proposed system increases with the rise in solar radiation, decreases with the rise in wind speed, and remains constant with the rise in ambient temperature and atmospheric emissivity.

Previous studies on RC of solar cells investigated the replacement of conventional glass cover with a spectrally selective radiator on top. The maximum solar cell temperature reduction achieved using such configuration was around 1°C to 2 °C, since glass has an inherently high emissivity. In contrast, by using the PV-HP-RC system proposed in this study, convective and radiative heat transfer from both the PV and RC module happens simultaneously, and thus a significant cell temperature reduction (~10 °C) and efficiency increment (~5.5%) is achieved.

Acknowledgments

The authors would appreciate the support provided by the State Key Laboratory of Clean Energy Utilization (Open Fund Project No. ZJUCEU2020006).

References

1. Wang, R.Z. and T.S. Ge, *Advances in solar heating and cooling*. Woodhead publishing series in energy: Number 102. 2016: Elsevier.
2. Lu, X., et al., *Cooling potential and applications prospects of passive radiative cooling in buildings: The current state-of-the-art.* Renewable and Sustainable Energy Reviews, 2016. **65**: p. 1079-1097.
3. Santamouris, M., *Cooling the buildings – past, present and future.* Energy and Buildings, 2016. **128**: p. 617-638.
4. *Statistics Time Series - Trends in Renewable Energy*. 2021 [cited 2021 May, 1]; Available from: https://www.irena.org/Statistics/View-Data-by-Topic/Capacity-and-Generation/Statistics-Time-Series.
5. Javed, M.S., et al., *Solar and wind power generation systems with pumped hydro storage: Review and future perspectives.* Renewable Energy, 2020. **148**: p. 176-192.
6. Li, S., et al., *Numerical simulation of a novel pavement integrated photovoltaic thermal (PIPVT) module.* Applied Energy, 2021. **283**: p. 116287.
7. Skoplaki, E. and J.A. Palyvos, *On the temperature dependence of photovoltaic module electrical performance: A review of efficiency/power correlations.* Solar Energy, 2009. **83**(5).
8. Otth, D. and R. Ross. *Assessing photovoltaic module degradation and lifetime from long term environmental tests*. in *Inst. Environ. Sci. 29th Annual Meeting*. 1983. Los Angeles.
9. Ahmed, S., et al., *A review on the integration of radiative cooling and solar energy harvesting.* Materials Today Energy, 2021: p. 100776.
10. Raman, A.P., et al., *Passive radiative cooling below ambient air temperature under direct sunlight.* Nature, 2014. **515**(7528): p. 540-4.
11. Zeyghami, M., D.Y. Goswami, and E. Stefanakos, *A review of clear sky radiative cooling developments and applications in renewable power systems and passive building cooling.* Solar Energy Materials and Solar Cells, 2018. **178**: p. 115-128.
12. Huang, Z. and X. Ruan, *Nanoparticle embedded double-layer coating for daytime radiative cooling.* International Journal of Heat and Mass Transfer, 2017. **104**: p. 890-896.
13. Ulpiani, G., et al., *On the energy modulation of daytime radiative coolers: A review on infrared emissivity dynamic switch against overcooling.* Solar Energy, 2020. **209**: p. 278-301.
14. Li, W., Y. Li, and K.W. Shah, *A materials perspective on radiative cooling structures for buildings.* Solar Energy, 2020. **207**: p. 247-269.
15. T., B. and L. A., *Fundamentals of Heat and Mass Transfer* 2017: Wiley.
16. Çengel, Y.A., *Heat Transfer: A Practical Approach*. 2004: New York : McGraw-Hill.
17. Lin, K.-T., et al., *Radiative cooling: Fundamental physics, atmospheric influences, materials and structural engineering, applications and beyond.* Nano Energy, 2021. **80**.
18. Zhao, B., et al., *Radiative cooling: A review of fundamentals, materials, applications, and prospects.* Applied Energy, 2019. **236**: p. 489-513.
19. Zhao, D., et al., *Radiative sky cooling: Fundamental principles, materials, and applications.* Applied Physics Reviews, 2019. **6**(2).
20. Zhu, L., et al., *Radiative cooling of solar cells.* Optica, 2014. **1**(1).
21. Zhu, L., A.P. Raman, and S. Fan, *Radiative cooling of solar absorbers using a visibly transparent photonic crystal thermal blackbody.* Proc Natl Acad Sci U S A, 2015. **112**(40): p. 12282-7.
22. Wu, S.H. and M.L. Povinelli, *Solar heating of GaAs nanowire solar cells.* Opt Express, 2015. **23**(24): p. A1363-72.
23. Safi, T.S. and J.N. Munday, *Improving photovoltaic performance through radiative cooling in both terrestrial and extraterrestrial environments.* Opt Express, 2015. **23**(19): p. A1120-8.
24. Perrakis, G., et al., *Passive radiative cooling and other photonic approaches for the temperature control of photovoltaics: a comparative study for crystalline silicon-based architectures.* Opt Express, 2020. **28**(13): p. 18548-18565.

25. Li, W., et al., *A Comprehensive Photonic Approach for Solar Cell Cooling.* ACS Photonics, 2017. **4**(4): p. 774-782.
26. Sun, X., et al., *Optics-Based Approach to Thermal Management of Photovoltaics: Selective-Spectral and Radiative Cooling.* IEEE Journal of Photovoltaics, 2017. **7**(2): p. 566-574.
27. Riverola, A., et al., *Mid-infrared emissivity of crystalline silicon solar cells.* Solar Energy Materials and Solar Cells, 2018. **174**: p. 607-615.
28. Mellor, A., et al., *Roadmap for the next-generation of hybrid photovoltaic-thermal solar energy collectors.* Solar Energy, 2018. **174**: p. 386-398.
29. Gentle, A.R. and G.B. Smith, *Is enhanced radiative cooling of solar cell modules worth pursuing?* Solar Energy Materials and Solar Cells, 2016. **150**: p. 39-42.
30. Sato, D. and N. Yamada, *Review of photovoltaic module cooling methods and performance evaluation of the radiative cooling method.* Renewable and Sustainable Energy Reviews, 2019. **104**: p. 151-166.
31. Zhao, B., et al., *Performance analysis of enhanced radiative cooling of solar cells based on a commercial silicon photovoltaic module.* Solar Energy, 2018. **176**: p. 248-255.
32. Li, Z., S. Ahmed, and T. Ma, *Investigating the Effect of Radiative Cooling on the Operating Temperature of Photovoltaic Modules.* Solar RRL, 2021. **5**(4).
33. Ahmed, S., et al., *A comparative performance evaluation and sensitivity analysis of a photovoltaic-thermal system with radiative cooling.* Solar Energy Materials and Solar Cells, 2021. **221**.
34. Esen, M. and H. Esen, *Experimental investigation of a two-phase closed thermosyphon solar water heater.* Solar Energy, 2005. **79**(5): p. 459-468.
35. Esen, M., *Thermal performance of a solar cooker integrated vacuum-tube collector with heat pipes containing different refrigerants.* Solar Energy, 2004. **76**(6): p. 751-757.
36. Yang, F., X. Yuan, and G. Lin, *Waste heat recovery using heat pipe heat exchanger for heating automobile using exhaust gas.* Applied Thermal Engineering, 2003. **23**(3): p. 367-372.
37. Alizadeh, H., et al., *Numerical simulation of PV cooling by using single turn pulsating heat pipe.* International Journal of Heat and Mass Transfer, 2018. **127**: p. 203-208.
38. Makki, A., et al., *Numerical investigation of heat pipe-based photovoltaic–thermoelectric generator (HP-PV/TEG) hybrid system.* Energy Conversion and Management, 2016. **112**: p. 274-287.
39. Du, Y., *Advanced thermal management of a solar cell by a nano-coated heat pipe plate: A thermal assessment.* Energy Conversion and Management, 2017. **134**: p. 70-76.
40. Shittu, S., et al., *Comparative study of a concentrated photovoltaic-thermoelectric system with and without flat plate heat pipe.* Energy Conversion and Management, 2019. **193**: p. 1-14.
41. Gang, P., et al., *Performance study and parametric analysis of a novel heat pipe PV/T system.* Energy, 2012. **37**(1): p. 384-395.
42. Alizadeh, H., et al., *Numerical analysis of photovoltaic solar panel cooling by a flat plate closed-loop pulsating heat pipe.* Solar Energy, 2020. **206**: p. 455-463.
43. Ezekwe, C.I., *Performance of a heat pipe assisted night sky radiative cooler.* Energy Conversion and Management, 1990.
44. Wang, Z., et al., *Lightweight, Passive Radiative Cooling to Enhance Concentrating Photovoltaics.* Joule, 2020. **4**(12): p. 2702-2717.
45. Zhai, Y., et al., *Scalable-manufactured randomized glass-polymer hybrid metamaterial for daytime radiative cooling*, in *Science*. 2017.
46. Zhao, B., et al., *Conventional photovoltaic panel for nocturnal radiative cooling and preliminary performance analysis.* Energy, 2019. **175**: p. 677-686.
47. Zhao, B., et al., *Performance evaluation of daytime radiative cooling under different clear sky conditions.* Applied Thermal Engineering, 2019. **155**: p. 660-666.
48. John A. Duffie, W.A.B., *Solar Engineering of Thermal Processes*. Fourth Edition ed. 2013: WILEY.

49. Lee, H., *Thermal Design: Heat Sinks, Thermoelectrics, Heat Pipes, Compact Heat Exchangers, and Solar Cells* 2010: John Wiley & Sons.
50. Shabgard, H., et al., *Heat pipe heat exchangers and heat sinks: Opportunities, challenges, applications, analysis, and state of the art.* International Journal of Heat and Mass Transfer, 2015. **89**: p. 138-158.
51. COMSOL *Heat Transfer Module User's Guide*. 2019.
52. COMSOL. *Application Gallery*. Available from: https://www.comsol.ch/models/heat-transfer-module/page/2?sort=popularity.
53. Zhao, B., et al., *Comprehensive photonic approach for diurnal photovoltaic and nocturnal radiative cooling.* Solar Energy Materials and Solar Cells, 2018. **178**: p. 266-272.
54. [cited 2020 7th, June]; Available from: https://energyplus.net/weather.